ICHEP'96 Ref. pa01-020
Submitted to Pa 01, 02, 04
Pl 02, 04, 05

DELPHI 96-68 CONF 2
25 June, 1996

Measurement of the Triple Gluon Vertex from double quark tagged 4-Jet Events

Preliminary

DELPHI Collaboration

A. Seitz

Abstract

The 4-jet-events of the data of 1992, 1993 and 1994 are analysed to determine the contribution of the triple-gluon-vertex. Two of the four jets are tagged as jets from b- or c-quarks using transversal lepton momentum and lifetime information. This yields significant differences in the shape of the distributions of the observables for 4 jets from graphs involving double gluon bremsstrahlung, triple gluon vertex or secondary quark production. The two-dimensional distributions in the generalized Nachtmann Reiter angle Θ^*_{NR} and the opening angle of the two secondary jets are used to fit C_A/C_F, the ratio of the coupling strengh of the triple-gluon-vertex to that of gluon bremsstrahlung and N_C/N_A, the ratio of the number of quark colours to the number of gluons:

$$C_A/C_F = 2.51 \pm 0.27 \text{ and } N_C/N_A = 0.38 \pm 0.10$$

The results are in agreement with the values expected from QCD: $N_C/C_F = 2.25$ and $N_C/N_A = 0.375$.

1 Introduction

An essential feature of Quantum Chromodynamics (QCD) is the self-coupling of the gluons due to their colour charges. The 'triple-gluon vertex' is a direct consequence of the non-Abelian nature of this gauge theory. The large two-jet rate for medium jet energies at hadron colliders can be considered as direct evidence for gluon-gluon scattering [1], if one accepts the extrapolation of the gluon structure function of the proton from deep-inelastic νN-scattering to collider energies. A colourless gluon would lead to the reaction $\Upsilon \to 2$ jets [2] which is not observed [3]. In e^+e^- annihilation the energy dependence [4] of the strong coupling constant α_s, where the triple gluon vertex enters through loop corrections, constitutes further indirect evidence. Direct evidence can be obtained from the study of 4-jet events in e^+e^- annihilation, since in four-parton final states the triple-gluon vertex contributes to the Born diagrams. Additional contributions to the 4-jet rate at Born-level originate from several classes of diagrams, e.g. ones with double gluon bremsstrahlung or diagrams in which a radiated gluon splits into $q\bar{q}$ pairs (secondary $q\bar{q}$ production).

In a previous analysis of 4-jet events [6] [7] two-dimensional distributions have been studied. The generalized Nachtmann-Reiter angle θ^*_{NR} (fig. 2) [5] has been used since it distinguishes between two-gluon final states and secondary $q\overline{q}$-production. It is defined as the angle between the two jet-momentum vector differences $(\vec{p}_1 - \vec{p}_2)$ of the jets from the primary partons and $(\vec{p}_3 - \vec{p}_4)$ of the jets from the secondary partons. The additional observable, the angle between the two jets coming from the secondary partons, α_{34} (fig. 2), distinguishes between triple-gluon vertex and double-bremsstrahlung. The contribution from the triple-gluon vertex may be determined directly from the two-dimensional event distribution in these two observables.

The previous analysis used energetic ordering of the jets to distinguish between jets coming from primary and secondary partons. For only 42% of the events the two highest energetic jets are coming from primary quarks. This lead to a smearing of the distributions of the observables for the diagrams contributing to 4-jet events.

In this analysis the primary jets were tagged by exploiting the large lifetime and the semileptonic decay of the primary hadrons from heavy quarks, which lead to detectable secondary vertices or leptons with high transverse momenta. The higher purity of the tagging method resulted in large differences in the shape of the distributions of the observables for gluon bremsstrahlung, triple gluon vertex and secondary quark production and increased the sensitivity of the method.

2 Theoretical Basis

The triple-gluon vertex in e^+e^- annihilation appears in terms which are second order or higher in the strong coupling constant. The diagrams are shown in fig. 1 for double bremsstrahlung, triple gluon vertex and secondary $q\bar{q}$ production. Thus testing the triple-gluon vertex requires a study of 4-jet events. Jet 1 and 2 correspond to the primary partons, jet 3 and jet 4 correspond to the secondary partons.

The fundamental couplings are illustrated in fig. 3. The Casimir factors C_F, C_A, T_F are a measure the coupling strengths of gluon radiation from quarks, of the triple-gluon vertex, and of gluon splitting into a quark-antiquark pair respectively. For any representation of a gauge group describing these couplings, they are determined in terms

of its generators t^r_{ab} and its structure constants f^{rst} by the relations (the notation of T. Hebbeker [8] is used):

$$t^r_{ab}t^r_{bc} = \delta_{ac}C_F \qquad \text{where:}$$
$$f^{rst}f^{rsu} = \delta^{tu}C_A \qquad a,b,... = \quad 1,....,N_C \quad \text{quark color index}$$
$$t^r_{ab}t^s_{ba} = \delta_{rs}T_F \qquad r,s,... = \quad 1,....,N_A \quad \text{gluon color index}$$

and repeated indices are to be summed.

The ratio of the coupling strength T_F for $g \to q\bar{q}$ to C_F for $q \to qg$ is then given by [10]:

$$T_F/C_F = N_C/N_A$$

The interference terms contain combinations of these basic couplings and this leads to more complicated graphs for the transition probabilities. The graphs can be grouped as simple planar ones and the more complicated nonplanar graphs where particle lines cross. R.K. Ellis et al. [9] have calculated the differential cross sections for the production of the four-parton final states in order α_s^2. In figs. 6 and 8 of their paper, all topologically distinct graphs for the transition probabilities are shown. For the $q\overline{q}gg$ final state there are 36 contributions which can be grouped into three classes:

A: planar double-bremsstrahlung graphs with weight C_F^2;

B: non-planar double-bremsstrahlung graphs with weight $C_F(C_F - \frac{1}{2}C_A)$;

C: graphs involving the triple-gluon vertex with weight C_FC_A.

Similarily the 36 contributions for $q\overline{q}q\overline{q}$ fall into the classes:

D: planar graphs with weight C_FT_R;

E: non-planar graphs with weight $C_F(C_F - \frac{1}{2}C_A)$;

F: graphs with weight C_F, which give contributions only if the charge of the partons is determined experimentally and are therefore not relevant to this analysis.

T_R and T_F and related by

$$T_R = T_F\, n_f$$

where n_f is the number of active quark flavours.

The original factor N_C in these expressions has been replaced by C_A, since this is the relevant coupling for the triple-gluon vertex [10]. In SU(N_C) gauge theory and in particular in QCD, the quantities C_A and N_C are equal. In other gauge groups however the different physical meaning of these factors results in different numerical values.

The differential cross section for 4-jet production in e^+e^- annihilation can be written in the form:

$$\sigma_4(y_{ij}) = \sigma_{q\bar{q}gg}(y_{ij}) \; + \; \sigma_{q\bar{q}q\bar{q}}(y_{ij})$$

Above and in the following text (y_{ij}) symbolizes the dependence on all the kinematical invariants $y_{ij} = m_{ij}^2/s \quad (i,j = 1,..,4)$, the normalised effective masses squared for any pair of jets (partons).

$$\sigma_{q\bar{q}gg}(y_{ij}) = \sigma_0 \; \alpha_s^2 \; C_F^2 \; \left[F_A(y_{ij}) + (1 - \tfrac{1}{2}\tfrac{\mathbf{C_A}}{\mathbf{C_F}})F_B(y_{ij}) \; + \tfrac{\mathbf{C_A}}{\mathbf{C_F}}F_C(y_{ij})\right]$$

$$\sigma_{q\bar{q}q\bar{q}}(y_{ij}) = \sigma_0 \; \alpha_s^2 \; C_F^2 \; \left[\tfrac{\mathbf{T_R}}{\mathbf{C_F}}F_D(y_{ij}) + (1 - \tfrac{1}{2}\tfrac{\mathbf{C_A}}{\mathbf{C_F}})F_E(y_{ij})\right]$$

where σ_0 is the zeroth order 2 parton cross section.

The kinematical functions $F_A, ..., F_E$ correspond to the distributions for the classes A,...,E, for which the formulae are given in ref. [9]. These formulae are also used for matrix-element simulation in the JETSET-Monte-Carlo-Program.

Grouping the contributions with respect to the Casimir-factors leads to:

$$\sigma_4(y_{ij}) = \sigma_0 \; \alpha_s^2 \; C_F^2 \; \left[F_{CF}(y_{ij}) + \tfrac{\mathbf{C_A}}{\mathbf{C_F}}F_{CA}(y_{ij}) + \tfrac{\mathbf{T_R}}{\mathbf{C_F}}F_{TR}(y_{ij}) \; \right]$$

where

$$\begin{aligned} F_{CF}(y_{ij}) &= F_A(y_{ij}) + F_B(y_{ij}) + F_E(y_{ij}) \\ F_{CA}(y_{ij}) &= F_C(y_{ij}) - \frac{1}{2}(F_B(y_{ij}) + F_E(y_{ij})) \\ F_{TR}(y_{ij}) &= F_D(y_{ij}) \end{aligned}$$

For QCD the fermionic Casimir operator is $C_F = \frac{4}{3}$, the coupling strength of the triple-gluon vertex $C_A = 3$ and $T_F = \frac{1}{2}$. For the Abelian model the values are $C_F = 1$, $C_A = 0$, $T_F = 3$ and for QED $C_F = 1$, $C_A = 0$, $T_F = 1$. The values for N_C/N_A and C_A/C_F in other gauge groups are given in table 1 [10]. Since the dependence on the Casimirs is gauge invariant, one can determine the ratios C_A/C_F and T_R/C_F by fitting the shape of the distribution and use the results as a test of QCD and compare with the predictions of other gauge groups too.

In this analysis the contributions of the classes are considered as functions of two observables. One is as usual the generalised Nachtmann-Reiter angle θ^*_{NR}. This observable has the advantage that no cuts in opening angles are needed on the 4-jet sample. The second observable is the opening angle α_{34} of the jets from the secondary partons. The two observables of our analysis are illustrated in fig. 2. There is some correlation between θ^*_{NR} and α_{34}; the study is therefore performed by plotting the two-dimensional distribution in the angular observables.

3 Treatment of Data and b-quark-tagging

The analysis is based on the data of 1992, 1993 and 1994 of multihadron events from e^+e^- annihilations at c.m.s. energies around the Z^0 resonance. Hadronic decays, $Z^0 \to q\bar{q}$, were

selected requiring at least 5 charged particles. A detailed description of the DELPHI detector is found elsewhere [16].

Tracks were accepted if they had an impact parameter to the nominal interaction vertex below 5 cm in the transverse plane with respect to the beam axis and below 10 cm along the beam direction. They were kept only if the measured track length was above 50 cm. Both charged and neutral particles were used in the event reconstruction. Photons are reconstructed as neutral showers in the barrel electromagnetic calorimeter, the High Density Projection Chamber (HPC) or reconstructed as photon converted in the material in front of the TPC. Particles were required to have momenta greater than 100 MeV/c.

The event was accepted if the total visible energy was larger then 15 GeV and each of the hemispheres $\cos\theta > 0$ and $\cos\theta < 0$ contained more than 3 GeV visible energy. Furthermore, for all events the polar angle θ of the sphericity axis has to be between 40^0 and 140^0 and the total momentum imbalance below 20 GeV/c. Only particles in the $25^0 < \theta < 155^0$ region were used. Jets are defined with the algorithm LUCLUS provided with the LUND Monte Carlo program [15], called JETSET. In this algorithm two jets with trimomenta values p_1, p_2 and opening angle α_{12} are merged together if $2\frac{p_1 * p_2}{p_1+p_2} * \sin\frac{\alpha_{12}}{2} \leq d_{join}$. Each time two jets are merged, new jet-axes are determined and all particles are reassigned to the nearest jet. With the new jets so defined, the procedure is repeated until a stable configuration is reached. The jet resolution parameter d_{join} is set to a fixed value of 4 GeV. An event was excluded if a single photon carried more than 70 % of the jet energy. This yields 20239, 19580 and 41367 4-jet events from the data of the three years.

To determine the influence of the DELPHI-detector, special matrix-element events with full simulation of the DELPHI detector have been used. Based on four parton final states 23340 4 jets (1992) and 6848 4 jets (1993) have been produced. Based on 2-, 3- and 4-parton final states 4058 4 jets (1992) and 70888 4 jets (1994) have been simulated. The background to 4 jet events coming from less than 4 partons was studied with this matrix-element simulation.

For later calculation of reference distributions the weights W_A, W_B, W_C for each qqgg-event and the weights W_D, W_E for qqqq-events as given in JETSET are stored.

Consistency between the simulated and the real data was checked by comparing their thrust distributions of 4 jet samples. Also the transverse particle momenta in the event plane with respect to the event axis, both defined by the sphericity tensor and the transverse particle momenta out of this plane were examined. For each of the jets 1 to 4 the distributions of jet momenta, of jet charged particle multiplicity and the transverse and longitudinal particle momenta relative to the jet axis were examined. The average values and width agree typically within about 3%.

For this analysis it is important to distinguish between jets coming from the primary quarks and jets coming from gluons or secondary quarks. In practice, these separations are possible only for heavy flavour decays, through the virtues of their large mass, long lifetimes, and distinctive decay modes. This separation is most effective for bottom quarks which have the largest mass and longest lifetimes. Gluon splitting in heavy quarks is suppressed. The methods to tag b-quarks group into two basic categories: those using semileptonic decays and those using lifetime information.

The semileptonic tagging consists of identifying leptons in hadronic Z^0 decays and making cuts on their P_t spectra.

Muon identification was based on an algorithm using a chi-squared fit, calculated from

the difference between the extrapolated track and the track element constructed with the hits in the muon chambers.

Electron identification was performed using an algorithm combining the information from the electromagnetic calorimeter HPC (deposited energy, longitudinal shape of the shower) and the dE/dx measurement from the TPC.

For the determination of the transversal momentum the lepton was excluded from the jet and the new jet direction was calculated.

The lifetime method uses the fact that the finite lifetime of B-hadrons leads to decay products with large impact parameters. This quantity was defined as the distance of closest approach between the charged-particle track and the Z-production point. This results in a distribution of impact parameters that is characteristically larger in jets containing a B-Hadron than in jets without. A probability was calculated for the whole event and for each jet separately that all the well-measured tracks belonging to the event or jet originate from the main vertex (compatible with the beam spot).

A combination of the methods lifetime-tag, lepton-tag and energetic ordering was done using a neural network. Input variables were the tranversal momentum of the electrons in each jet, the transversal momentum of the muons in each jet, the four lifetime probabilities for each jet and the event lifetime-probability. The network had four output nodes, one for each jet. Output node one was the node of the highest energetic jet and so on. Therefore energetic ordering is also included. A jet was tagged as a primary quark jet when the corresponding output variable had a value higher 0.5. An event was accepted if two of the four jets were tagged. The net was trained with matrix element monte carlo. In the training sample the jet with the smallest angle to the parton was the corresponding jet.

Selecting only those events which passed the multihadron selection, seen as a 4 jet event with two tagged jets yields in 5794 data events and 4707 simulated events (full ME 1992: 559 events, 4 parton ME 1992: 3402 events and 4 parton ME 1993: 746 events) and for 1994 in 6795 data events and 12121 simulated events. The tagging method results in an efficiency to tag both of the two primary jets correctly of $11.85 \pm 0.13\%$ and a purity of $69.97 \pm 0.7\%$ for 1994.

4 Analysis

4.1 Fit of the Casimir-factors

The 4-jet events from the data are sorted into a 8 x 8 matrix according to their values of $|\cos\theta^*_{NR}|$ and $\cos\alpha_{34}$ for 1992/93 and 1994 seperately to consider the upgrade of the Vertexdetector. The theoretical predictions are prepared as two-dimensional reference distributions $R_{CF}(l,m)$, $R_{CA}(l,m)$ and $R_{TR}(l,m)$ in the form of 8 x 8 matrices in $|\cos\theta^*_{NR}|$ and $\cos\alpha_{34}$ which were produced from JETSET 7.3 generator using the second order ERT Matrix Element followed by a full simulation of the DELPHI detector. The theoretical prediction for the number of 4-jets is then given for each bin l,m by:

$$T(l,m) = Norm \left[R_{CF}(l,m) + \frac{\mathbf{C_A}}{\mathbf{C_F}} * \frac{R_{CA}(l,m)}{2.25} + \frac{\mathbf{T_R}}{\mathbf{C_F}} * \frac{R_{TR}(l,m)}{1.875} \right]$$

where $Norm$ is the overall normalisation factor. The denominators 2.25 and 1.875 take into account that the reference distributions are produced with the nominal QCD-values

of C_A/C_F and T_R/C_F. The two-dimensional reference distributions are shown in fig. 4 and fig. 5.

The data is compared to

$$P(l,m) = T(l,m) + F(l,m)$$

where $F(l,m)$ represents the background to the 4-jet events from fragmentation fluctuations of three and two parton events. Its contribution has been determined from the full-simulation of detector effects with the complete QCD matrix element and amounts to $1.35 \pm 0.45\%$ of the 4-jet events. This background has a sizeable influence as its shape (see fig. 4) is completely different from the reference distributions.

A χ^2-fit was then performed to the $|\cos\theta^*_{NR}|$ vs α_{34} distribution in terms of the two variables $X_1 = \frac{\mathbf{C_A}}{\mathbf{C_F}}$, and $X_2 = \frac{\mathbf{T_R}}{\mathbf{C_F}}$, using MINUIT [15] for minimisation. From a combined fit of both variables, the relative contribution of the three classes can be separated.

4.2 Details of the Fitting Procedure

The available statistics with full simulation of detector effects is not larger than the number of events in the data. Moreover the reference distributions $R_{CF}(l,m)$, $R_{CA}(l,m)$ and $R_{TR}(l,m)$ cannot be generated directly on an event by event basis, since for some (y_{ij}) configurations $W_{CA}(y_{ij})$ becomes negative.

$q\bar{q}gg$-events and $q\bar{q}q\bar{q}$- events are generated as usual in JETSET and followed through the detector simulation and tagging procedure. This gave 4288 events from $q\bar{q}gg$ and 410 events from $q\bar{q}q\bar{q}$. For calculation of reference distributions for each qqgg-event the weights W_A, W_B, W_C and for qqqq-events the weights W_D, W_E as given in JETSET are also written out. The reference distributions are obtained by splitting these events according to their relative weights and filling each event into the reference-distributions with these relative weights.

For each event i the following quantities are calculated:

$$\begin{aligned}
W_{gg}(i) &= C_F * (F_A(i) + F_B(i)) + C_A * (-0.5 * F_B(i) + F_C(i)) \\
W_{CF}(i) &= C_F * (F_A(i) + F_B(i))/W_{gg}(i) \\
W_{CA}(i) &= (C_A * (-0.5 * F_B(i) + F_C(i))/W_{gg}(i) \\
W_{q\bar{q}}(i) &= T_R * F_D(i) + (C_F - 0.5 * C_A) * F_E(i) \\
W_{TR}(i) &= T_R * F_D(i)/W_{q\bar{q}}(i) \\
W_E(i) &= (C_F - 0.5 * C_A) * F_E(i)/W_{q\bar{q}}(i),
\end{aligned}$$

where $C_F = 4/3$ and $C_A = 3$ are the nominal QCD-values.

The reference distributions are obtained by summing over the $q\bar{q}gg$- and $q\bar{q}q\bar{q}$-events in each bin l,m:

$$\begin{aligned}
R_{CF} &= \sum_{i=1}^{N_{gg}} W_{CF}(i) + \sum_{i=1}^{N_{q\bar{q}}} W_E(i)) \\
R_{CA} &= \sum_{i=1}^{N_{gg}} W_{CA}(i) - 0.5 * \sum_{i=1}^{N_{q\bar{q}}} W_E(i))
\end{aligned}$$

$$R_{TR} = \sum_{i=1}^{N_{q\bar{q}}} W_{TR}(i))$$

Also the squares of the weights are sorted for each event into histograms. They allow to calculatate the elements of the variance matrix for R_{CF}, R_{CA} (class E contributes only about 0.3 % to the events; the influence is neglected here):

$$\begin{aligned} v_{CF}v_{CF} &= \sum_{i=1}^{N_{gg}} W_{CF}(i)^2 \\ v_{CA}v_{CA} &= \sum_{i=1}^{N_{gg}} W_{CA}(i)^2 \\ v_{CF}v_{CA} &= 0.5 * \sum_{i=1}^{N_{gg}} (1 - W_{CF}(i)^2 - W_{CA}(i)^2) \qquad since \quad W_{CF}(i) + W_{CA}(i) = 1 \end{aligned}$$

The reference distributions R_{CF} and R_{CA} have some correlations, since they originate from the same events. With the covariance matrix this can be taken correctly into account.

The background of 4-jet events coming from fragmentation fluctuations of three and two-parton evnets is included with the propagation of its statistical error. The influence of the background is therefore included in the total statistical error.

In the standard fits only 55 bins of the 8 x 8 matrix are used. The 8 bins in the row near $\cos\alpha_{34} = 1$ are omitted. Also omitted is the bin in the corner $|\cos\theta^*_{NR}| = 1$, $\cos\alpha_{34} = -1$. These bins contain only few events and are not adequate for a χ^2-fit. They are also at the boundaries of the two-jet resolution and therefore less reliable in the simulation.

5 Systematic Errors

5.1 Influence of the bin selection

To test the stability of the fit values, one row of bins and a bin in one corner for the 1992/93 analysis have been added or omitted. This changed the χ^2 of the fit from 74.04 (62 d.o.f.) to 58.45 (53 d.o.f). The change for C_A/C_F is 0.14 and for T_R/C_F 0.35. There is no indication of a significant systematic influence caused by different bin selections around the standard 55 accepted bins.

5.2 Background from three and two parton events

If the background from 3- and 2-parton events is 'switched off' totally, there are changes of $\Delta(C_A/C_F) = 0.1$ and $\Delta(T_R/C_F) = 0.32$. The background and its statistical error is included in the fit procedure and therefore part of the total statistical error.

5.3 Fragmentation

To study the influence of the variation of the fragmentation parameters on the results, the five fragmentation parameters a, b, σ_q, ϵ_c, ϵ_b have been choosen independently

in a large range around their nominal values by a random generator. The same large sample of 4-parton events was used to study the fragmentation for each set of parameters and a simple b-tag-algorithm and a simple detector simulation was included on generator level. The fragmentation was done for 500 different sets of parameters. The sets were then considered as data, and fit values for C_A/C_F and T_R/C_F have been determined. The values of C_A/C_F and T_R/C_F for the sets were compared with those from 500 sets generated with the nominal fragmentation parameters. The rms shifts in the two parameters including a one sigma error were 0.11 and 0.25, respectively.

5.4 Influence of higher orders

It is not possible to give a quantitative estimate of the influence of higher orders. Only the tree contributions in the next order α_s^3 are available and included in event generators. The internal loop-corrections to the 4-parton final state have not yet been calculated. If QCD is the correct theory then the agreement of this analysis with the QCD-values can be interpreted as an indication that the influence of the higher orders is relatively small.

5.5 Influence of heavy quark masses

The production of secondary heavy quark-antiquark pairs is kinematicly suppressed. The quark tagging algorithm rises the ratio of secondary heavy flavours again. A seperate study with the applied jet cut has shown that the different flavours are generated in the ratio $d : u : s : c : b = 1 : 1 : (1.11 \pm 0.06) : (1.5 \pm 0.07) : (1.95 \pm 0.07)$. The effective number of active quark flavours is then $n_f^{eff} = 6.56 \pm 0.12$. This number is already built into the reference distributions, which are used in the fit. Since the number of secondary quarks is know to be 5 one has to divide by 5 to reduce the result for T_R/C_F to the value T_F/C_F for one quark flavour.

The ERT matrix element includes the effects of quark masses only on kinematics but not on the angular structure of the event. The OPAL collaboration investigated the effect with generators including this mass effect [17]. It was found that the mass effect does not influence the result on C_A/C_F and introduces only a small uncertainty for T_R/C_F.

5.6 Dependence of the Y_{cut}

In the calculations of the parton cross-sections a y_{cut} is applied to handle the divergencies from soft and collinear gluons. On the parton level $y_{cut} = 0.01$ in the generator is below the cut imposed on the kinematical configuraton by the value of d_{join} in the LUCLUS cluster routine. When lowering the y_{cut} additional softer partons are produced, but after applying the cut criteria of the cluster routine on the parton configuration exactly the same parton events survive. This independence on the y_{cut} is not perfect for the jets from the hadrons due to fluctuations in the fragmentation of the partons.

The influence of the change in the y_{cut} on the result of the analysis has been determined by generating 50 samples of events with the $y_{cut} = 0.11, 0.12$ and 0.14. This was done using the same simple b-tagging algorithm as for the fragmentation study. The events were fitted against the real data. There was no significant shift in respect to the nominal $y_{cut} = 0.10$ result.

5.7 Dependence of the Cluster–Algorithm

To investigate the influence of the cluster–algorithm the analysis was done several times using the LUCLUS and the YCLUS algorithm with different values for d_{join} and y_{cut}. The results of these fits vary within the statistic error of our nominal fit with the standard d_{join} of 4.0 GeV. Therefore no additional systematic error was included.

6 Discussion and Conclusions

The combined fit results of 1992/93 and 1994 are

$$C_A/C_F = 2.51 \pm 0.25\,(stat.) \pm 0.11\,(fragm.)$$

$$T_R/C_F = 1.91 \pm 0.44\,(stat.) \pm 0.25\,(fragm.)$$

where $T_R = n_f\,T_F$. The last error is the systematic uncertainty from the fragmentation parameters. Since $T_F/C_F = N_C/N_A$, and $n_f = 5$, one can obtain the ratio for the number of quark colours N_C to the number of gluon colours N_A. Adding the errors in quadrature results in

$$C_A/C_F = 2.51 \pm 0.27 \qquad \text{and} \qquad N_C/N_A = 0.38 \pm 0.10$$

The result for C_A/C_F is in agreement with the value 9/4 expected for QCD. The value for N_C/N_A is consistent with the QCD value of 3/8.

The measured variables C_A/C_F and N_C/N_A represent the ratios of the coupling strength of the triple-gluon vertex to that of gluon bremsstrahlung from a quark, and of the number of quark colours to the number of gluons. The plot with the contours for 68 % and 95 % confidence levels is given in fig. 6.

The triple-gluon vertex must exist and that generally the number of quark colours has to be smaller than the number of gluons.

The expectations for various other gauge groups are given in fig. 10. The quarks are assumed to be in the fundamental representation and the gluons in the adjoint representation, except for SU(4)‘, SP(4)‘, and SP(6)‘, which are examples with quarks in the next higher representation.

From table 1 it is evident that most groups in the plot are excluded by their inherent number of quark colours which is also restricted experimentally to $N_C = 3$ by the hadronic cross section in e^+e^--annihilation ususally expressed as $R = \sigma\,(e^+e^- \to hadrons)\,/\,\sigma\,(e^+e^- \to \mu^+\mu^-)$ and the decay width of the π^0 into two photons via quark loops.

Apart from SU(3) and the ad hoc invented Abelian model $U(1)_3$, only SO(3) has 3 colours for the quarks, but only 3 gluons in contrast to QCD which has 8 gluons. Our result excludes SO(3) as a candidate and establishes that 8 gluons exist in nature.

References

[1] L. DiLella, Ann. Rev. Nucl. Part. Sci. 35 (1985) 107

[2] T.F. Walsh and P.M. Zerwas, Phys. Lett. 93B (1980) 53

[3] ARGUS Collaboration, H. Albrecht et al., Z. Physik C31 (1986) 181

[4] S. Bethke: Plenary talk at the Dallas 1992-Conference

[5] G. Rudolph, Physics at LEP, CERN 86-02 (1986) Vol. 2, 150

[6] DELPHI Collaboration, P. Abreu et al., Phys. Lett. 255B (1991) 466

[7] DELPHI Collaboration, P. Abreu et al., Z. Physik C59 (1993) 357

[8] T. Hebbeker, Tests of Quantum Chromodynamics in Hadronic Decays of Z^0 Bosons Produced in e^+e^- Annihilations, Phys. Rep. 217 (1992) 69

[9] R. K Ellis, D. A. Ross and A. E. Terrano, Nucl. Phys. B178 (1981) 421

[10] M. Jezabek, private communications

[11] M. Bengtsson, Z. Physik C42 (1989) 75

[12] S. Bethke, A. Ricker and P.M. Zerwas, Heidelberg-Aachen preprint PITHA 90/14

[13] DELPHI Collaboration, P. Aarnio et al., Phys. Lett. 240B (1990) 271

[14] T. Sjöstrand, Computer Phys. Comm. 39 (1986) 347
T. Sjöstrand and M. Bengtsson, Computer Phys. Comm. 43 (1987) 367
LUCLUS is described in T. Sjöstrand, Computer Phys. Comm. 28 (1983) 229

[15] F. James and M.Roos, CERN library program D506 on GENLIB

[16] DELPHI Collaboration, NIM (1991) 233-276

[17] OPAL Collaboration, CERN-PPE/94-135

Table 1:

Expectation for the Observables in Different Gauge Theories

The quarks are assumed to be in the fundamental representation and the gluons in the adjoint representation, except for the lines marked with * where the quarks are in the next higher representation of this gauge group.

N_C/N_A=ratio of quark colours to number of gluons

C_A/C_F=ratio of coupling strength of triple-gluon vertex to gluon-bremstrahlung off quarks

Group	Gluons:	Quarks:	N_C/N_A	C_A/C_F
SU(n)	n^2-1	n	$\frac{n}{n^2-1}$	$\frac{2n^2}{n^2-1}$
*	n^2-1	$\frac{n(n-1)}{2}$	$\frac{n}{2(n+1)}$	$\frac{n^2}{(n+1)(n-2)}$
SO(n)	$\frac{n(n-1)}{2}$	n	$\frac{2}{n-1}$	$2-N_C/N_A$
Sp(2n)	$n(2n+1)$	2n	$\frac{2}{2n+1}$	$2+N_C/N_A$
*	$n(2n+1)$	$2n^2-n-1$	$1-1/n$	$2-N_C/N_A$
G_2	14	7	1/2	2
F_4	52	26	1/2	3/2
E_6	78	27	9/26	18/13
E_7	133	56	8/19	24/19
E_8	248	248	1	1
$U(1)_3$ Abelian	1	3	3	0
U(1) QED-like	1	1	1	0

Figure Captions

Fig. 1 Diagrams yielding four parton-final states

(a) Double-bremsstrahlung

(b) Secondary $q\overline{q}$ production

(c) Triple-gluon vertex

Fig. 2 Definitions of the generalised Nachtmann-Reiter angle θ^*_{NR} in terms of the jet momentum vectors $\vec{p}_j$, and of the angle α_{34} used in this analysis to distinguish the triple-gluon vertex contribution from that due to double-bremsstrahlung (The index j increases with decreasing jet momentum).

Fig. 3 Casimir factors for the fundamental couplings.
Diagrams (a) and (c) have the same topology; the coupling strenghts are related to the numbers of quark colours N_C and gluons N_A by $T_F/C_F = N_C/N_A$.

Fig. 4 Two-dimensional distributions in $|\cos\theta^*_{NR}|$ and $\cos\alpha_{34}$ of the Monte–Carlo–Simulation for 1994

(a) Reference distribution R_{CF}

(b) Reference distribution R_{CA}

(c) Reference distribution R_{TR}

(d) background of 3 parton events seen as 4 jets

Fig. 5 Box plot of the distributions in $|\cos\theta^*_{NR}|$ and $\cos\alpha_{34}$

(a) Reference distribution R_{CF}

(b) Reference distribution R_{CA}

(c) Reference distribution R_{TR}

(d) DELPHI-Data

Fig. 6 68 % CL and 95 % contour plots for the measured variables C_A/C_F and N_C/N_A, and expections from different gauge theories

C_A/C_F = ratio of coupling strength of $g \to gg$ to $q \to qg$
N_C/N_A = number of quark colours divided by the number of gluons
It is evident that the triple-gluon vertex must exist and that generally the number of quark colours has to be smaller than the number of gluons.

Quarks are in the fundamental and gluons in the adjoint representation (except SU(4)', SP(4)', SP(6)', where the quarks are in the next higher representation). Most groups have $N_C \neq 3$ (see table 1) and are already excluded by $N_C = 3$ from $R = \sigma(e^+e^- \to hadrons)/\sigma(e^+e^- \to \mu^+\mu^-)$ and $\Gamma(\pi^0 \to \gamma\gamma)$. $N_C = 3$ only for the Abelian model $U(1)_3$, SO(3), and QCD. Our result excludes SO(3) as a candidate.

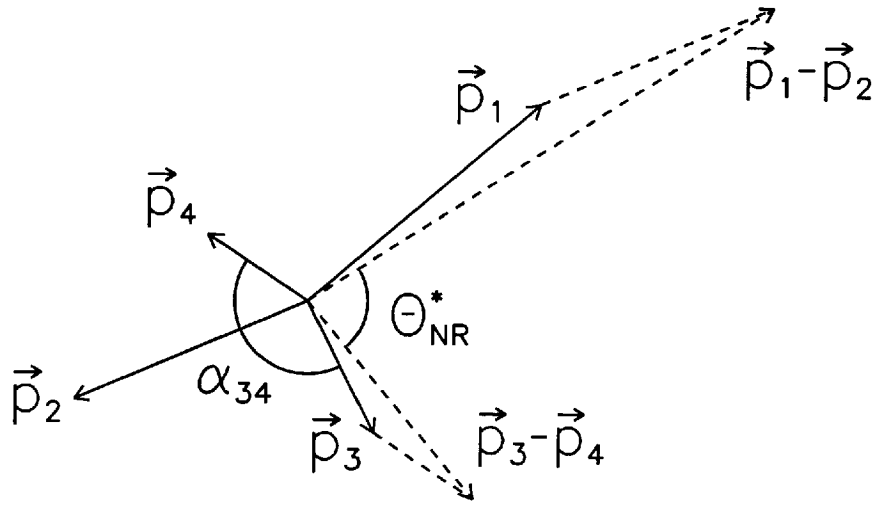
$\vec{p}_1$
$\vec{p}_1-\vec{p}_2$
$\vec{p}_4$
Θ^*_{NR}
α_{34}
$\vec{p}_2$
$\vec{p}_3$
$\vec{p}_3-\vec{p}_4$

Figure 1:

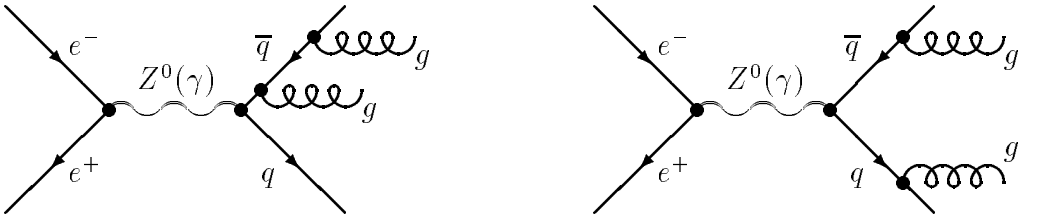
e^-
e^+
$Z^0(\gamma)$
$\overline{q}$
q
g
g
e^-
e^+
$Z^0(\gamma)$
$\overline{q}$
q
g
g

(a)

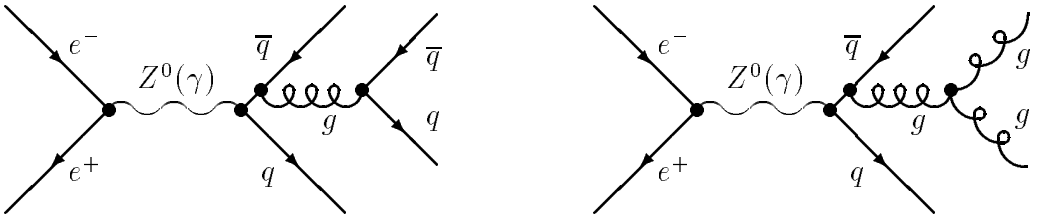
e^-
e^+
$Z^0(\gamma)$
$\overline{q}$
q
g
$\overline{q}$
q
e^-
e^+
$Z^0(\gamma)$
$\overline{q}$
q
g
g
g

(b) **(c)**

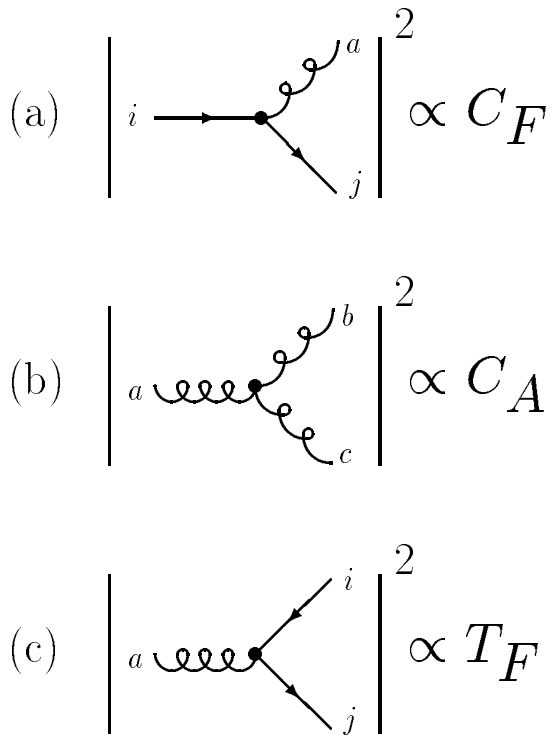

Figure 3:

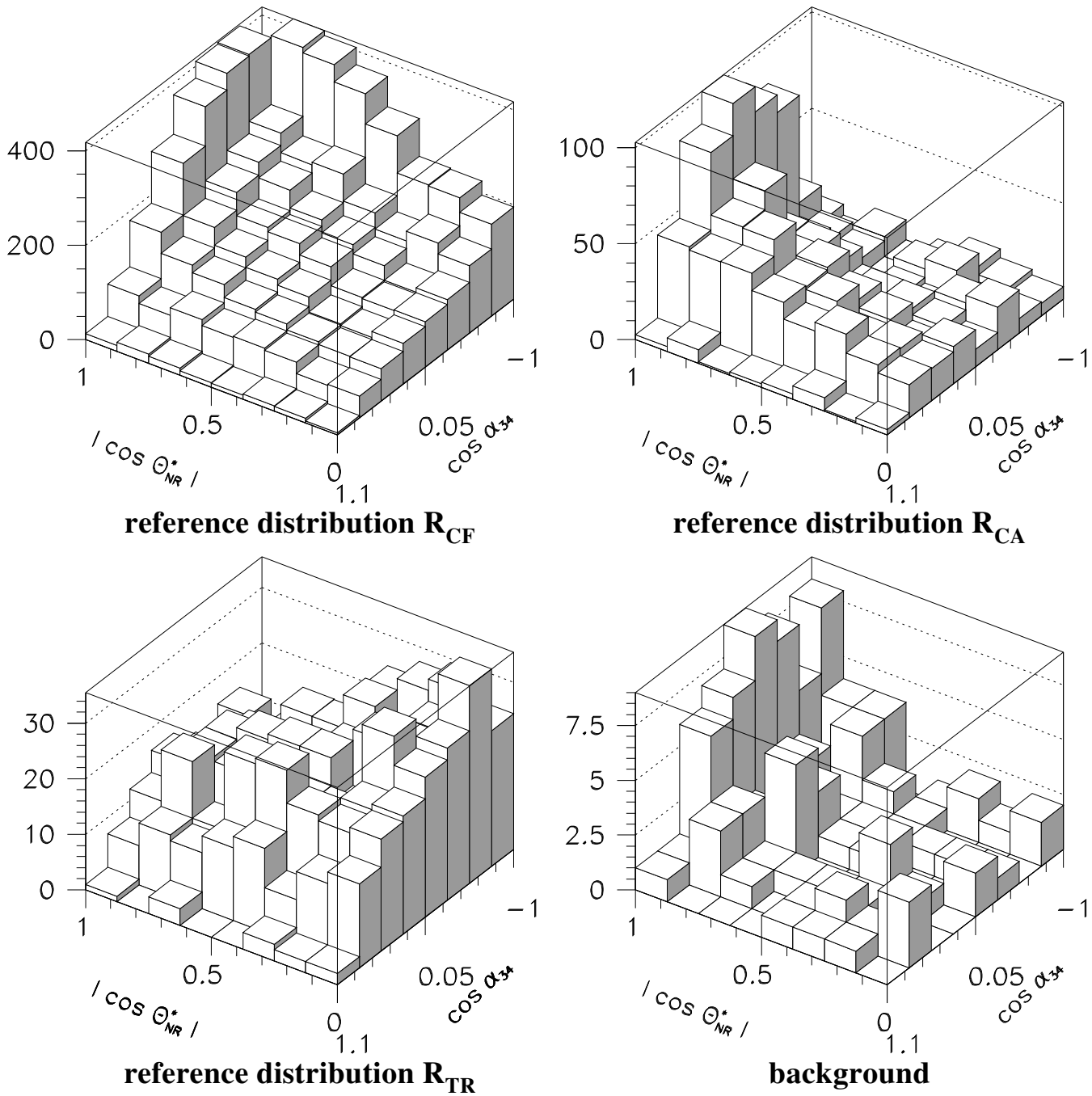
400
200
0
1
0.5
0
/ cos Θ*NR /
1.1
0.05
cos Θ-34
−1
reference distribution RCF
100
50
0
1
0.5
0
/ cos Θ*NR /
1.1
0.05
cos Θ-34
−1
reference distribution RCA
30
20
10
0
1
0.5
0
/ cos Θ*NR /
1.1
0.05
cos Θ-34
−1
reference distribution RTR
7.5
5
2.5
0
1
0.5
0
/ cos Θ*NR /
1.1
0.05
cos Θ-34
−1
background

Figure 4:

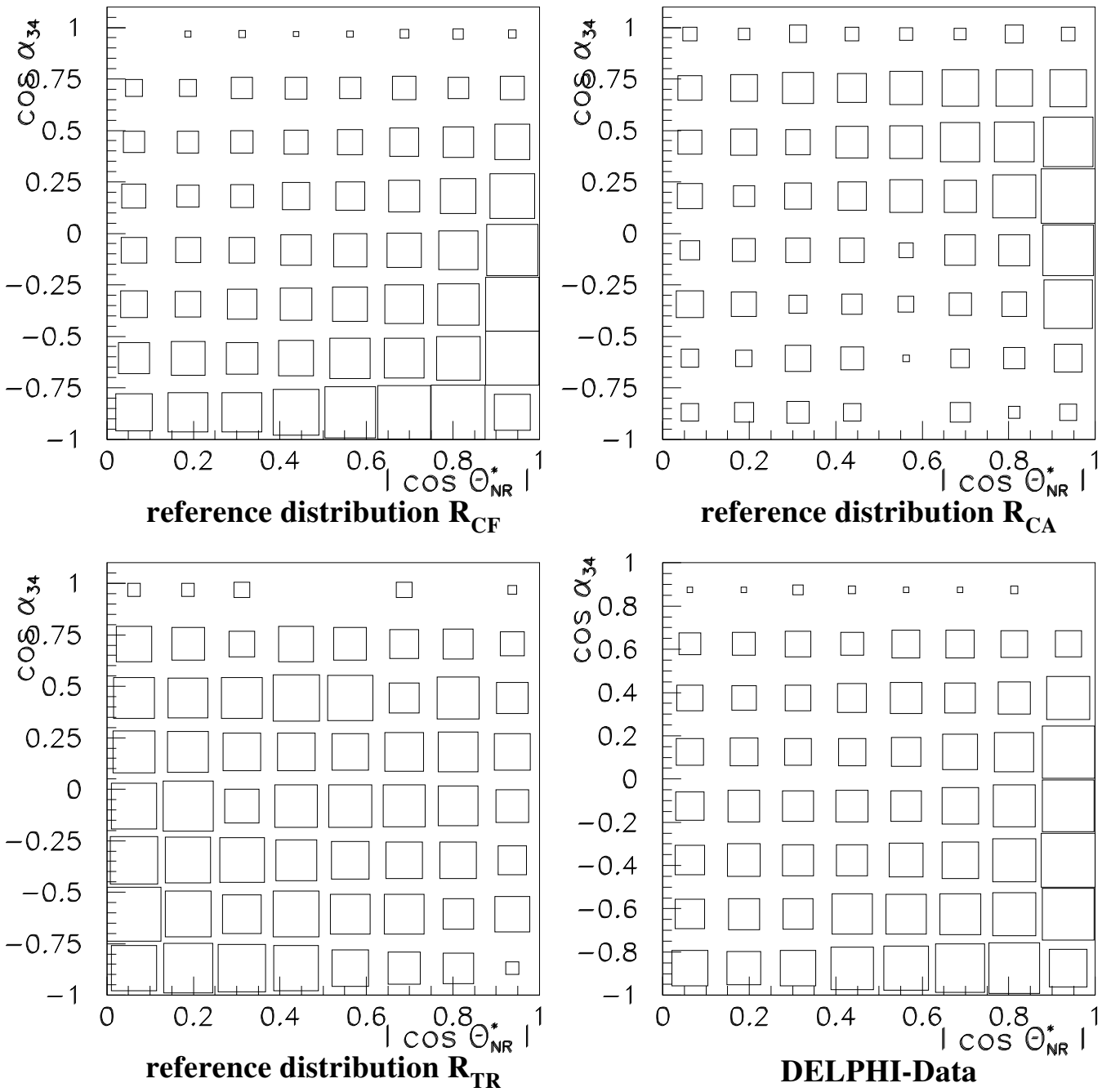
cos α34
| cos Θ*NR |
reference distribution RCF
reference distribution RCA
reference distribution RTR
DELPHI-Data

Figure 5:

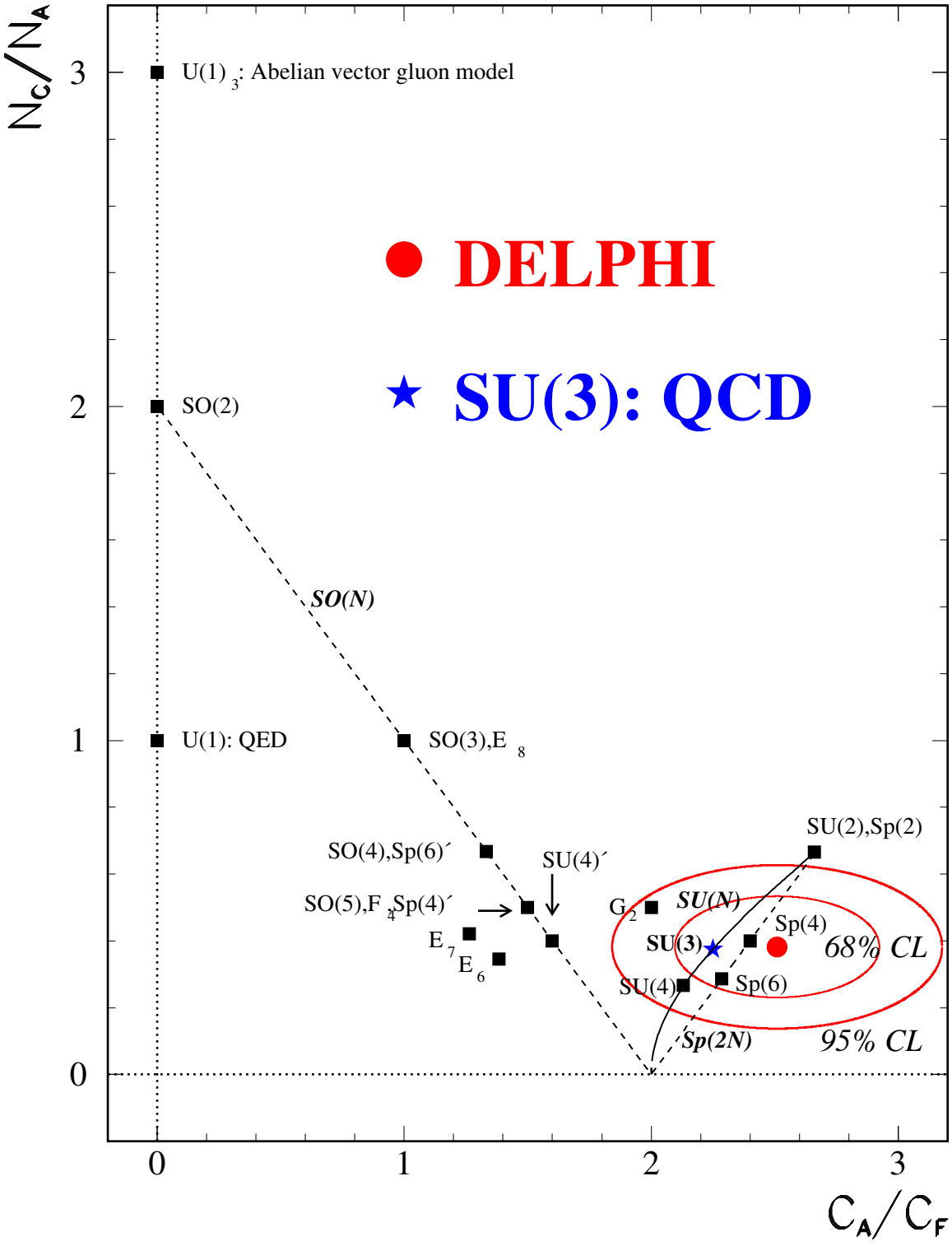
N_C/N_A
3
2
1
0
U(1) $_3$: Abelian vector gluon model
DELPHI
SU(3): QCD
SO(2)
SO(N)
U(1): QED
SO(3),E $_8$
SO(4),Sp(6)´
SU(4)´
SO(5),F $_4$Sp(4)´
E $_7$
E $_6$
SU(2),Sp(2)
G $_2$
SU(N)
Sp(4)
SU(3)
68% CL
SU(4)
Sp(6)
Sp(2N)
95% CL
0
1
2
3
C_A/C_F

Figure 6: